

Accepted Manuscript

Electrodeposition and magnetic properties of three-dimensional bulk and shell nickel mesostructures

F. Nasirpouri, S.J. Bending, L.M. Peter, H. Fangohr

PII: S0040-6090(11)00714-0
DOI: doi: [10.1016/j.tsf.2011.03.058](https://doi.org/10.1016/j.tsf.2011.03.058)
Reference: TSF 29094

To appear in: *Thin Solid Films*



Please cite this article as: F. Nasirpouri, S.J. Bending, L.M. Peter, H. Fangohr, Electrodeposition and magnetic properties of three-dimensional bulk and shell nickel mesostructures, *Thin Solid Films* (2011), doi: [10.1016/j.tsf.2011.03.058](https://doi.org/10.1016/j.tsf.2011.03.058)

This is a PDF file of an unedited manuscript that has been accepted for publication. As a service to our customers we are providing this early version of the manuscript. The manuscript will undergo copyediting, typesetting, and review of the resulting proof before it is published in its final form. Please note that during the production process errors may be discovered which could affect the content, and all legal disclaimers that apply to the journal pertain.

Electrodeposition and magnetic properties of three-dimensional bulk and shell nickel mesostructures

F Nasirpouri^{a,*}, S. J. Bending^b, L. M. Peter^c, H. Fangohr^d

^a Department of Materials Engineering, Sahand University of Technology, Tabriz
51335-1996, Iran

^b Department of Physics, University of Bath, Bath BA2 7AY, UK

^c Department of Chemistry, University of Bath, Bath BA2 7AY, United Kingdom.

^d School of Engineering Sciences, University of Southampton, Southampton SO17 1BJ,
United Kingdom.

In this paper we demonstrate the electrodeposition of nickel, a common ferromagnetic material, in various magnetically desirable shapes including nanowires, nanoparticles and highly faceted shells. In order to obtain three dimensional mesostructures, the electrochemical deposition of nickel was performed on highly oriented pyrolytic graphite (HOPG) under different electrolyte composition and deposition potential conditions. Under potentiostatic deposition at one distinct potential negative with respect to the reversible potential of nickel, three stages of nucleation and growth take place leading to a complex morphology of deposits. However, dual-pulse potential deposition and electrodeposition in low pH solutions causing hydrogen evolution, lead to nickel deposits in the form of nanowires and nanoparticles with the complete absence of a faceted morphology. Highly faceted nickel shells were electrodeposited via a dual-bath method on prefabricated silver mesocrystals electrodeposited on HOPG. Magnetic properties of faceted three dimensional nickel shells reveal clear signatures of mesocrystal facets of mesocrystals in the form of sharp steps in measured hysteresis loops and a strong magnetic anisotropy with respect to applied field direction.

Keywords: Electrodeposition, nickel, nanowires, nanoparticles, core-shell, magnetic

*- Corresponding author, email: Nasirpouri@sut.ac.ir

properties, micro-Hall probe.

1. Introduction

Controlling the shape of metallic mesostructures has been the subject of intensive research in recent years because it provides one with the ability to tune their magnetic and electronic properties [1-4]. Magnetic micro- or nanostructures have generally been fabricated by lithographic methods [5], in addition to some other well known routes for creating different shapes and size of magnetic structures such as template-based methods [6].

Electrodeposition is an effective method for growing structures with a range of sizes, from nanometers up to macroscopic dimensions. The growth mechanism of electrodeposits on a surface depends critically on the interaction strength between adatoms and the surface. It is possible to grow structures ranging from epilayers to three dimensional (3D) islands [7]. The electrodeposition of a metal onto a highly oriented pyrolytic graphite (HOPG) surface occurs via a Volmer–Weber mechanism [8,9] in which three-dimensional nuclei are readily formed. It has recently been reported that 'architecture-tuneable' three dimensional (3D) Pb mesostructures can be grown by electrodeposition from simple aqueous solutions [10-12] onto HOPG substrates. Simply by varying the reduction potential an extraordinary variety of possible morphologies ranging from regular polyhedra and nanowires to multipods and 'snowflakes' could be realized. Until now, electrodeposition and magnetic properties of highly faceted ferromagnetic mesocrystals have not been reported. Prior reports have only provided an understanding of the nucleation and growth mechanism [13,14]. It is therefore important to investigate this area as the development of regular and faceted three dimensional ferromagnetic crystals by electrodeposition may lead to rich new

physical phenomena. The effect of the shape of ferromagnetic crystals is quite interesting and relatively little explored. For example, it is well known that domain walls can be pinned at corners [15] and constrictions [16] in multipod or star-shaped structures yielding multistable magnetisation states which should be readily observable. The goal of this work is to controllably fabricate regular faceted 3D nickel ferromagnetic mesocrystals and study their magnetic properties. Different electrodeposition conditions were investigated in order to engineer the morphology of the nickel mesostructures. General electrodeposition of Ni on HOPG and two deposition techniques including dual-step and hydrogen co-evolution assisted deposition techniques were investigated leading to different shaped regular 3D nickel mesostructures. A hybrid method is also demonstrated here to successfully produce highly faceted 3D nickel magnetic shells on top of a silver mesocrystal ‘template’.

2. Experimental

Electrodeposition was performed in a conventional three-electrode cell connected to a computer-controlled potentiostat/galvanostat instrument (microAutolab III). Commercially available HOPG (grade 1 from SPI Supplies) was used as a working electrode in a horizontal orientation inside the cell. A platinum plate was used as counter electrode. A standard Ag/AgCl electrode and high-purity silver wire were used as reference electrodes for electrodeposition of nickel and silver, respectively. Electrolytes were prepared by dissolving laboratory grade chemicals into deionized water with a resistivity value of 18 M Ω .cm. Electrolytes for nickel plating were deaerated for 10 min with de-humidified N₂ prior to use. To obtain appropriate deposition potentials, cyclic voltammograms were taken in the different electrolytes.

To fabricate bulk nickel mesostructures, the electrochemical deposition was performed

in potentiostatic mode using the chronoamperometry technique, during which the current transients were recorded while, for three-dimensional shell films of nickel, a two-step dual-bath method was used to electrodeposit silver-nickel core-shell structures on HOPG working electrodes at ambient temperature. Electrodeposition of nickel was carried out from different electrolytes and Table 1 shows the electrolyte compositions used. For the dual-bath method the following procedure was used: in the first step, highly faceted silver mesocrystals were electrodeposited from an aqueous electrolyte containing 100 mM of Ag nitrate in water at a pH between 2 and 2.5. The value of pH was adjusted by adding nitric acid into the primary solution containing simple nitrate salt. After depositing silver, the sample was then gently rinsed in deionized water and blow dried with argon. In the second step nickel was electrodeposited from a Watt's bath, as indicated in Table 1. The thickness of nickel shell was estimated from Faraday's law using the computer-controlled deposition software (Autolab-GPES). For the given surface area of the working electrode and the effective surface density of silver islands, the nickel thickness was estimated to be 100 nm from the known total charge of 4 mC that passed through the cell. Here the cathodic current efficiency of nickel was assumed to be 100%. Scanning electron microscopy (SEM model Hitachi 4300S), energy dispersive x-ray spectroscopy (EDS) and atomic force microscopy (AFM model Asylum research MFP-3D) were used to characterize the morphology and structure of the grown materials.

M_z - H_z magnetisation measurements were carried out at 5K using a linear array of $2\mu\text{m} \times 2\mu\text{m}$ GaAs/AlGaAs heterostructure Hall probes (H_z is the field applied perpendicular to the plane of the Hall sensors and M_z is the measured component of magnetisation in the same direction). Individual core-shell structures were removed from the working

electrode and placed on top of one of the active Hall elements using a piezoelectric nanomanipulator under a high magnification optical microscope. Mesostructures were fixed to the arrays with a low melting temperature paraffin wax such that the base of the pyramid was in direct contact with the sensor with the apex pointing upwards (called the z-direction) and parallel to the surface of Hall probe (called the x-direction). The Hall probes were operated with a $20\mu\text{A}$ 32Hz ac current and the Hall voltage detected with a lock-in amplifier. An external magnetic field, H_z , was applied perpendicular to the plane of the Hall array and the square base of the Ag-Ni structures using a superconducting solenoid.

3. Results and Discussion

3.1. General behavior of electrodeposition of nickel on HOPG

Cyclic voltammograms taken from dilute electrolyte (solution 1) and the Watts bath (solution 2), show that nickel reduction occurs at more negative potentials on the first potential sweep. However, nickel start to deposit on HOPG at less negative potentials with lower nickel content (solution 1a – not shown here due to space limitations). A typical cyclic voltammogram is shown in Figure 1 for the deposition and dissolution of nickel from the Watts bath. The semi-reversible behavior of the electrodeposition of nickel indicates it can be deposited more easily on the second potential sweep due to the breakdown of the nucleation barrier on HOPG [13].

Current transients recorded during electrodeposition of nickel from dilute and Watts solutions (Figure 1b) clearly show that a three-stage nucleation and growth mechanism takes place, arbitrarily divided on the graphs. The general mechanism of the electrodeposition of nickel from sulphate solutions on vitreous carbon substrates shows the typical behavior described earlier by Abyaneh et al [17] including: (i) the deposition

of a monolayer of nickel via two-dimensional nucleation and crystal growth under special conditions accompanied by hydrogen evolution on both the edges and tops of the growth centers, (ii) three dimensional nucleation and crystal growth on top of the first monolayer and (iii) the overlap of growth centers initiated in the last parts of stage ii followed by outward growth into the solution, which can be associated with the death of the initial growth centers and the rebirth of new growth centers by further nucleation. Figure 2 illustrates SEM images of the progress of the three stages of electrodeposition of nickel on HOPG at infinite deposition times solely to recognize the three-stages. The first stage described above can be negligible for the electrodeposition of metallic centers on HOPG as there is no evidence of any rise in current at the beginning of the current transient. This may be because of the very low surface energy of HOPG and the low bonding energy between the metal atoms and the substrate [13,14]. After a certain time, the current starts to increase implying that Ni particles are being readily formed, as shown on Fig 2a. However, nucleation occurs preferentially at step edges on the graphite surface. In the case of metal atoms residing on HOPG surfaces, step edge selectivity is promoted due to its ability to catalyze electron transfer to metal ions in solution [18-19]. Previously, it has been demonstrated that the threshold required for nucleation at steps is smaller than the nucleation on terraces [20]. As illustrated in Figures 2b and 2c, when the deposition process continues for long enough, the coalescence of nickel centers at step edges and also terraces occurs (i.e., stage (ii)) until the centers start to overlap (stage iii). At this point, overgrown nickel is found to form. Figure 2d shows the overlapped nickel centers indicating the destructive effects of hydrogen evolution on grown centers. The simultaneous H_2 reduction is evident from the dark circles sporadically created by H_2 bubbles growing on the electrode surface.

The Ni deposit can also be observed under the evolving bubbles, which indicates catalytic reduction of H₂ by deposited Ni [21].

3.2. Electrodeposited nickel mesostructures in the form of nanowires and nanoparticles

As seen, the electrodeposition of nickel from sulphate solutions at a distinct potential reveals that particles and wires of nickel are formed at step edges and terraces, but this is not a reliable method for the production of individual magnetic mesostructures. The morphology evolution of nickel mesostructures was investigated by changing the electrodeposition conditions in two ways including: dual-step potentiostatic deposition and lowering the pH value leading to co-evolution of hydrogen.

3.2.1. Electrodeposition of nickel nanowires

In the dual-step potentiostatic deposition method, two potentiostatic pulses were applied in rapid succession. The first is a nucleation pulse lasting just 5 ms and having a deposition potential of -850 mV versus Ag/AgCl. This pulse produces “seed” nanoparticles pseudorandomly on the graphite surface. Immediately following the nucleation pulse, a growth voltage pulse with a deposition potential of -580 mV versus Ag/AgCl is applied lasting up to a minute [8]. As shown in the cyclic voltammogram in Figure 1a for nickel, the potential of this growth pulse is at the beginning of the nickel reduction peak in the cyclic voltammogram acquired on freshly cleaved HOPG. At this potential, the rate of nucleation is exceedingly slow, so the dual pulse has the added benefit of enforcing a separation between nucleation and growth in time. If the nucleation pulses are omitted, the nucleation density along step edges would be low on average and metal nanowires are not obtained. The selection of the growth potential is critical and involves a compromise because values of this potential that are too negative

cause the nucleation and growth of metal particles on terraces, whereas values that are too positive can cause the rate of nanowire growth to be depressed to the point where several hours are required. The optimization of nucleation and growth for each metal, and each metal plating solution, involves considerable trial and error [13,14,20].

This dual pulse method produces a high nucleation density along step edges. With continued growth, this dense linear array of metal nuclei evolves into a continuous nanowire with a diameter of 50 nm or so [14]. Figure 3 shows SEM and AFM images of nickel nanowires, electrodeposited with the dual-pulse method, indicating that nanowires are deposited on step edges of HOPG. At the current conditions of electrodeposition, nickel is deposited in the form of a nanowire having a diameter of about 120 (± 3.45) nm, shown in the inset to Figure 3a. The length of the nanowires produced with this technique was observed to be more than 20 micrometers with a uniform diameter along the wire axis.

3.2.2. Electrodeposition of Nickel nanoparticles

In the next electrodeposition technique, we also employed a low pH Watts solution to produce Ni nanoparticles by exploiting the co-evolution of H_2 during reduction of Ni^{2+} . This method has been introduced earlier by Penner and co-workers [14] using nickel nitrate solution at high pH values which make an appreciable contribution of hydrogen evolution during nickel electrodeposition. Ni electrodeposition from sulfate supporting electrolytes at pH 2 and 4 has been investigated [21] and a strong influence of H_2 evolution and its effect on the morphology of Ni electrodeposits have been observed in this electrolyte at conditions indicating excess of H_3O^+ over Ni^{2+} , e.g., at pH 2. Our results clearly indicate the presence of hydrogen evolution in a Watts bath with a low pH value of 2. The electrode in this experiment is partially covered with hydrogen

bubbles that are visible to the eye. In the cyclic voltammograms acquired in the negative direction, separate peaks for nickel deposition and H₂ evolution were not observed because a significant barrier to the nucleation of nickel exists on graphite. The contribution of hydrogen evolution to the current passed through the cell is higher when the deposition potential approaches more negative values [14,21]. The deposition potential, and hence the H₂ coevolution rate, strongly influences the morphology of electrodeposited nickel structures on HOPG. This effect is seen in the scanning electron microscopy (SEM) images of Figures 3c,d, which were obtained for nickel nanoparticles prepared using deposition potentials of -1.1 and -1.2 V versus Ag/AgCl from solution 3. The size of nickel particles measured from SEM images was 191.8 (\pm 13.1) nm and 414.38 (\pm 28.4) nm for the particles electrodeposited at -1.1 and -1.2 versus Ag/AgCl, respectively. It is also interesting to observe the narrow size distribution of nanoparticles electrodeposited due to hydrogen evolution. This has been described using Brownian dynamics simulations incorporating inhomogeneous diffusion-controlled nucleation and growth without interparticle coupling [14].

As is evident in the images, we clearly find a complete absence of facets on nickel mesostructures prepared using either dual-pulse deposition or low pH methods. The cause of this has been attributed to fact that these mesostructures are nanocrystalline. The formation of nanocrystalline nickel deposits with dual-pulse plating under high current densities has been well studied for many years [22]. The nanocrystalline nature of the nickel particles prepared from a nitrate solution has been characterized [8,14] using electron microscopy data.

3.3. Electrodeposition of highly faceted nickel shell mesostructures on HOPG

Although some studies have been performed on surface magnetism of textured magnetic

films, there has been very little research on faceted ferromagnetic crystals. Direct electrodeposition of nickel from aqueous solutions does not form highly faceted crystals, as we have also observed in our experiments. Therefore, we have used dual-bath electrodeposition to coat a thin magnetic shell layer of nickel on top of a highly faceted mesocrystal 'template' like silver. It has been shown that Ag can be deposited in the form of highly faceted hexagonal or truncated hexagonal crystals [23]. Using the same method, highly faceted silver hexagonal mesocrystals with different sizes and shapes were electrodeposited from silver nitrate solution. Figure 4 illustrates two types of electrodeposited Ag mesocrystals studied in this paper including (a) hexagonal Ag platelets electrodeposited at -60 mV in a solution of 0.6 M AgNO₃ for 5 sec and (b) truncated Ag polyhedra with 6-fold rotational symmetry electrodeposited at -70 mV in a solution of 0.1 M AgNO₃ for 20 sec. A Ni shell film with a nominal thickness of ~100 nm was then electrodeposited on silver mesocrystals from a Watts bath (solution 2) at a potential of -800 mV versus Ag/AgCl reference electrode. This value is estimated by counting the pre-electrodeposited silver metallic centers on HOPG, calculating the total surface of silver mesocrystals and applying the Faraday's law. On the basis of this calculation there is likely to be a substantial error bar on the nominal thickness value. Cyclic voltammograms taken from the Watts bath on freshly cleaved HOPG and silver electrodeposited HOPG, showed a considerable deviation from the equilibrium potential of reduction of nickel ions to solid nickel. This is shown in the inset to Fig. 1a. When nickel is electrodeposited on the bare HOPG, it starts to reduce at potentials more negative than -840 mV versus Ag/AgCl reference electrode. In the presence of silver metallic centers on HOPG, the reduction of nickel is facilitated as it starts to grow at potentials more negative than -670 mV versus Ag/AgCl. At this

potential, the nucleation rate of nickel on HOPG is considerably slower and the nickel shell is solely electrodeposited on silver centers. The inset to Fig. 4a demonstrates the surface elemental distribution of nickel and silver, taken using the EDX analyzer, indicating that nickel is only detected on top of the silver mesocrystal. Surface roughening of the polycrystalline nickel shell is clearly seen, either as a result of the well established three-dimensional nucleation and growth mechanism of nickel electrodeposition [24] or due to the presence of hydrogen evolution [25] on the crystalline Ag core.

Magnetic hysteresis loops of individual Ni-Ag mesostructures, with the different shapes shown in Figs. 4a and 4b, were measured and reproduced in Figure 5. In Fig. 5a, the magnetization reversal of the hexagonal platelet structure exhibits regular coherent rotation of ferromagnetic moments as expected for an approximately thin film sample with in-plane anisotropy and no obvious facets. The same was true for all mesocrystals with this shape that were measured. The M_z value recorded at saturation for this structure seems to be greater in magnitude than the truncated 6-fold polyhedron shown in Figs 5b,c. We have examined different hexagonal platelet Ag-Ni core-shell mesocrystals and find that the measured saturation values of M_z do not seem to be systematically dependent on the crystal size. We assume then that the different values of M_z can be ascribed to deviations of the actual thickness of Ni shells from the nominal estimated values. Figures 5b,c show magnetization curves for the truncated 6-fold polyhedron measured for two different applied field directions. For the field applied along the z-direction we observe sharp steps in magnetisation reversal steps that appear to occur at characteristic values of applied field. We link these steps to the abrupt reversal of the faceted vertical sidewalls of the structure which have in-plane magnetic

anisotropy. A comparison of the magnetic behaviour to these two different-shaped structures clearly shows how magnetisation reversal can be tuned via shape control. The mechanism of magnetization of such highly faceted structures is not yet completely understood, but micromagnetic simulations carried out on simpler scaled-down pyramidal-shaped Ni-Ag structures exhibit the formation of several stable and metastable states among which magnetic vortex states are prominent in larger structures [26]. In this case sweeping the magnetic field makes it possible to switch the magnetic state abruptly between two vortex states, leading to kinks in the magnetisation curves. We are currently performing large scale micromagnetic simulations to understand the behavior of the structures measured here. Switching events could, for example, occur via the nucleation and propagation of domain walls that are pinned at structural defects or geometrically ‘trapped’ due to the shape of the mesostructures [27,28]. Previous studies [29] of the growth of Ni nanostructures on HOPG have revealed that Ni has a nanocrystalline nature with FCC lattice and it would be reasonable to expect the same structure in our nickel film shells. We find that the specific Ni microstructure does not influence the observed step-wise magnetic behavior, and presume that arises due to shape anisotropy in our thin films.

Conclusion

Magnetic properties of individual mesostructures are of great interest in order to develop novel applications. Nickel mesostructures with different shapes ranging from nanowires and nanoparticles to faceted shell films, have been electrodeposited on HOPG. A ferromagnetic nickel shell was electrodeposited onto silver mesocrystals with hexagonal platelet and truncated 6-fold polygon shapes. Measured magnetization curves of these two structures show a smooth rotation of magnetic moments for the hexagonal

platelet and abrupt steps in M_z for highly faceted truncated 6-fold polygons which are related to very different characteristic magnetization reversal modes in the two cases.

Acknowledgements

We acknowledge financial support for this work from the Engineering and Physical Sciences Research Council (EPSRC) in the U.K. under grant numbers EP/E039944/1 & EP/E040063/1 and from the European Community's Seventh Framework Programme (FP7/2007-2013) under Grant Agreement n° 233552 (DYNAMAG project) .

References

- [1] C. Burda, X. Chen, R. Narayanan, M. A. El-Sayed, Chem. Rev., Chem. Rev. 105 (2005) 1025.
- [2] A. K. Geim, S. V. Dubonos, J. J. Palacios, I. V. Grigorieva, M. Henini, J. J. Schermer, Phys. Rev. Lett., 85 (2000) 1528.
- [3] M. Morelle, J. Bekaert, V. V. Moshchalkov, Phys. Rev. B, 70 (2004)094503.
- [4] A. Kanda, B.J. Baelus, F.M. Peeters, K. Kadowaki, Y. Ootuka, Phys. Rev. Lett. 93, (2004) 257002 .
- [5] I. Martin, J. Nogues, K. Liu, J.L. Vicent, I. K. Schuller, J. Magn. Magn. Mater., 256 (2003) 449.
- [6] F. Nasirpouri, "Template electrodeposition of magnetic nanowire arrays: A review", Editor: A. El-Nemr, Research Signpost Publications, pp 51-93, 2007.
- [7] L. Péter and I. Bakonyi, Electrodeposition as a fabrication method for magnetic nanostructures, in F. Nasirpouri and A. Nogaret (Eds.), Nanomagnetism and spintronics, World Scientific Publishing Co, Singapore (2010), pp. 89-120.

- [8] H. Liu, F. Favier, K. Ng, M.P. Zach, R.M. Penner, *Electrochimica Acta* 47 (2001) 671
- [9] R. M. Penner, *J. Phys. Chem. B* 2002, 106, 3339.
- [10] Z.L. Xiao, C.Y. Han, W.K. Kwok, H. Wang, U. Welp, J. Wang, G. W. Crabtree., *J. Am. Chem. Soc.*, 126 (2004) 2316.
- [11] A. E. Muller, S. E. C. Dale, M. A. Engbarth, S. J. Bending, L. M. Peter, *CrystEngComm*, 12 (2009) 2135.
- [12] Sara E. C. Dale, Simon J. Bending, L. M. Peter, 25 (2009) 11228–11231.
- [13] E. C. Walter, B. J. Murray, F. Favier, G. Kaltenpoth, M. Grunze, and R. M. Penner, *J. Phys. Chem. B*, 106 (2002) 11408.
- [14] P. Zach , R. M. Penner, *Adv. Mater.*, 12 (2000) 878.
- [15] T. Taniyama et al, *Phys. Rev. Lett*, 82 (1999) 2780.
- [16] G. Tatara et al, *Phys. Rev. Lett.*, 83 (1999) 2030.
- [17] M.Y. Abyaneh, M. Fleischmann, *J. Electroanal. Chem.*, 119 (1981) 187.
- [18] Bowling, R. J.; McCreery, R. L.; Pharr, C. M.; Engstrom, R. C., *Anal. Chem.* 1989, 61, 2763.
- [19] Robinson, R. S.; Sternitzke, K.; McDermott, M. T.; McCreery, R.L. *J. Electrochem. Soc.* 138 (1991) 2412.
- [20] Zach, M. P.; Inazu, K.; Hemminger, J. C.; Penner, R. M. *Chem. Mater.* 14 (2002) 3206.
- [21] M. Streckova, R. Orinakova, R. Rozik, L. Trnkova, M. Galova, *Helvetica Chimica Acta*, 89 (2006) 622.
- [22] A. M. El-Sherik, U. Erb, J. Page, *Surf. Coat. Technol.* 88 (1996) 70.
- [23] G. Hills, A.K. Pour., B. Scharifker, *Electrochimica Acta*, 28 (1983) 891.

- [24] A. Saraby-Reintjes and M. Fleischmann, *Electrochimica Acta*, 29 (1984) 557-566.
- [25] W Schwarzacher *J. Phys.: Condens. Matter* 16 (2004) R859
- [26] A. Knittel, M. Franchin, T. Fischbacher, F. Nasirpouri, S. Bending, and H. Fangohr, *New Journal of Physics*, 12 (2010) 113048.
- [27] P. Bruno, *Phys. Rev. Lett.* 83 (1999) 2425 .
- [28] P. Haibach, M. Huth, H. Adrian, *Phys. Rev. Lett.* 84 (2000) 1312.
- [29] M.P. Zach, R. M. Penner, *Advanced Mater*, 12 (2000) 878.

Figure caption

Fig. 1. (a) A typical cyclic voltammogram taken in solution 2 (Watts bath) on a freshly cleaved HOPG at scan rate of 20 mV/sec. The inset to panel (a) shows a cyclic voltammogram taken in the same solution on silver electrodeposited HOPG demonstrating a more positive reduction potential. (b) Current transient recorded during one-step potentiostatic electrodeposition of nickel at -0.850 mV versus Ag/AgCl from solution 2 (Watts bath). Inset to panel b illustrates the current transient for electrodeposition of nickel at -0.850 versus Ag/AgCl from solution 1 (dilute).

Fig. 2. Scanning electron micrographs taken of nickel electrodeposited from a Watts bath (solution 2) at a potential of -0.850 V versus Ag/AgCl for (a) 5 sec, (b) 20 sec, (c) 75 sec and (d) 150 sec, representing the three stages of electrodeposition of nickel on HOPG.

Fig. 3. Effect of dual-pulse plating and pH value on the morphology of nickel mesostructures. (a) SEM image of nickel nanowires electrodeposited at -850 mV versus Ag/AgCl for 5 ms and -580 mV versus Ag/AgCl for 400 sec. Inset to (a) shows the

precise diameter of a typical nickel nanowire in a high magnification image. (b) Three dimensional AFM image shows the growth of one nickel nanowire with diameter of 100 nm. (c) and (d) SEM images of nickel nanoparticles electrodeposited at -1.1 and -1.2 V versus Ag/AgCl for 50 sec.

Fig. 4. SEM images of (a) a hexagonal platelet electrodeposited at -60 mV in a solution of 0.6 M AgNO₃ for 5 sec and (b) a truncated 6-fold symmetric Ag polygon electrodeposited at -70 mV in a solution of 0.1 M AgNO₃ for 20 sec. Ag cores have subsequently been plated with Ni in a Watts bath to create Ag-Ni core-shell mesocrystals. Insets to panel (a) show Ag and Ni elemental surface maps obtained from EDX analysis.

Fig. 5. Hysteresis loops measured using micro-Hall probe magnetometry of individual nickel-silver mesostructures. Panel (a) is for the mesostructure shown in Fig. 4a. Panels (b) and (c) are for the mesostructure shown in Fig. 4b, when the external magnetic field is applied along the base (x-direction) and apex (z-direction), respectively.

Table 1

Composition of different electrolytes used for electrodeposition of nickel mesostructures on HOPG at room temperature.

Solution number	Solution name	Ni Sulphate Molar/ L	Ni Chloride Molar/ L	Boric Acid Molar/ L	pH
		H ₂ O	H ₂ O	H ₂ O	
1	Dilute	0.1	-	0.2 M	3.4-3.8
2	Watt's bath	2.3	0.6	0.5	3.2-3.5
3	Watt's bath				2*

low pH

*- The value of pH was adjusted by addition of an adequate amount of sulphuric acid.

Fig. 1, Nasirpouri et al.

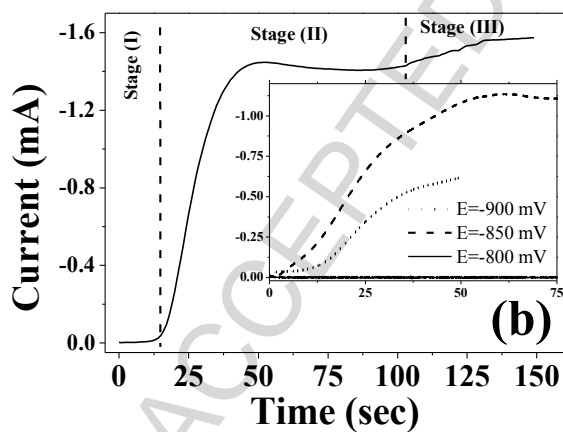
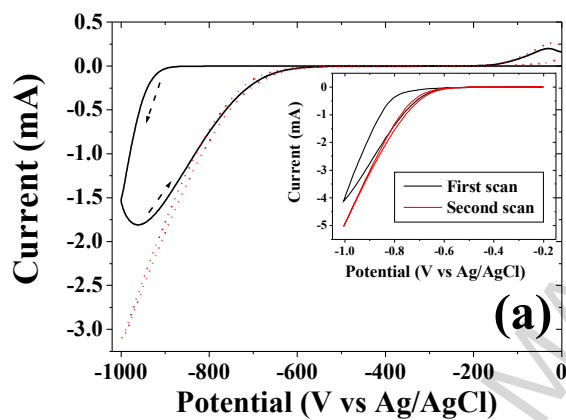


Fig. 2. Nasirpouri et al.

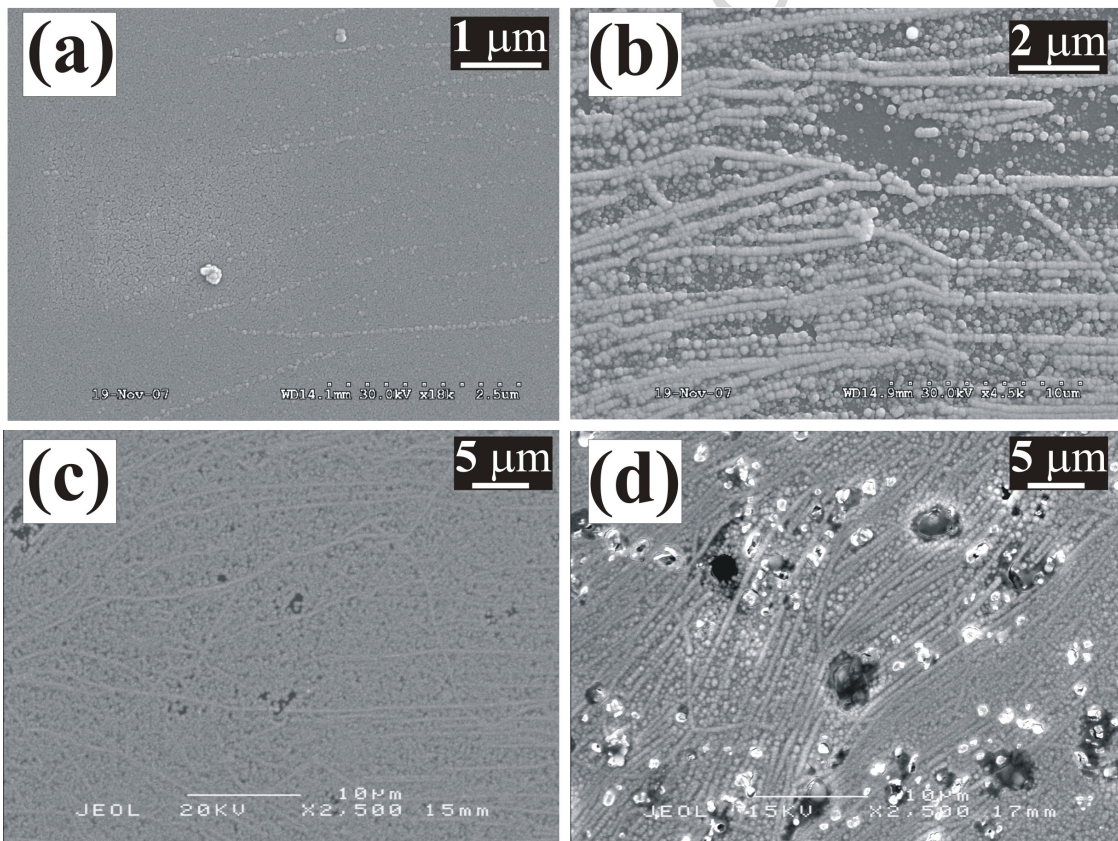


Fig 3 Nasirpouri et al.

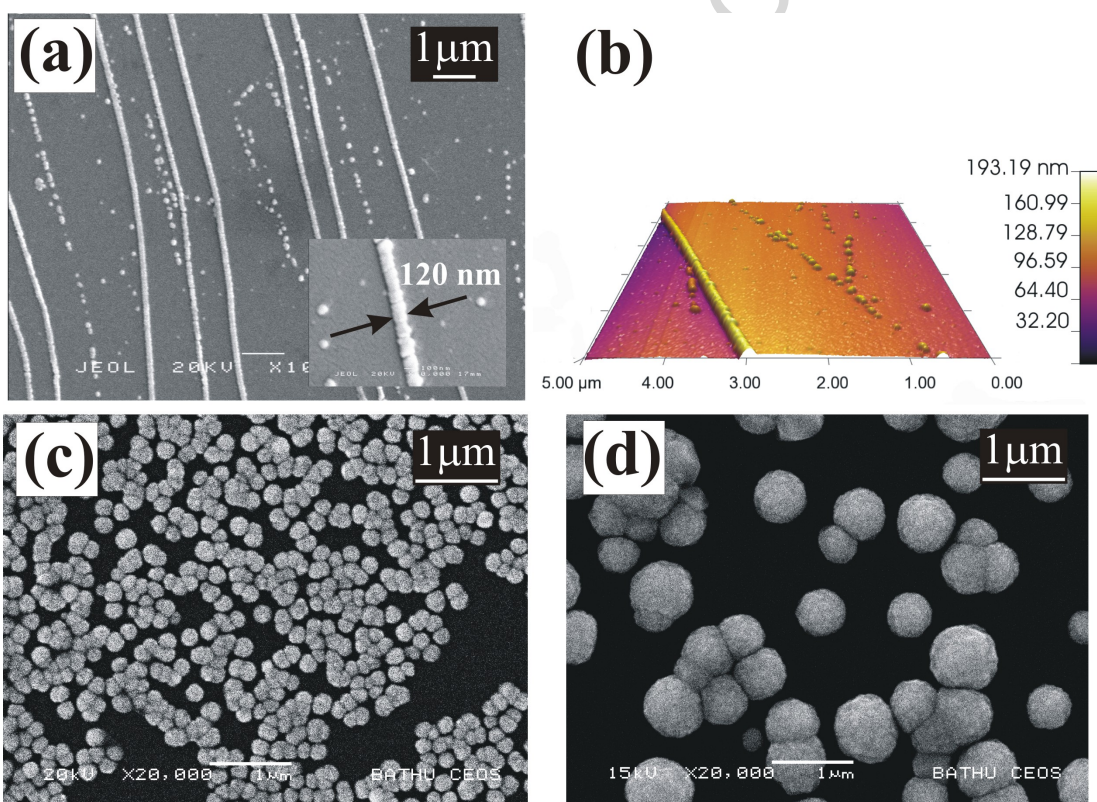


Fig 4. Nasirpouri et al.

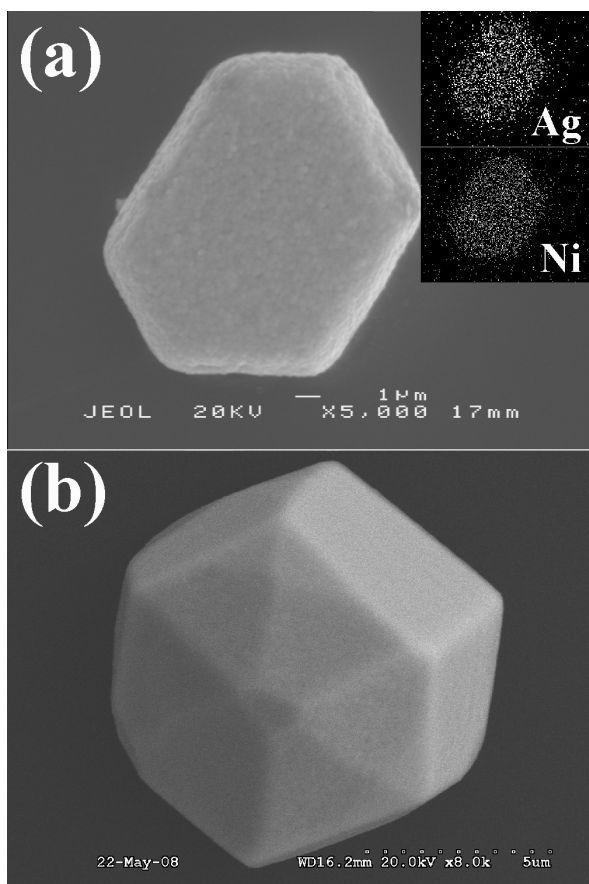


Fig. 5 Nasirpouri et al

